Eilenberger theory for nuclear magnetic relaxation rate in superconducting vortex lattice state

Kenta K. Tanaka,* Masanori Ichioka,† Seiichiro Onari, Noriyuki Nakai, and Kazushige Machida
Department of Physics, Okayama University, Okayama 700-8530, Japan
(Received 30 October 2014; revised manuscript received 7 January 2015; published 20 January 2015)

On the basis of the Eilenberger theory, spatial variation of the local NMR relaxation rate T_1^{-1} is quantitatively estimated in the vortex lattice state, to clarify the differences between the s-wave and the d-wave superconductors. We study the temperature and the magnetic field dependencies of T_1^{-1} inside and outside of the vortex core, including influences of nonmagnetic impurity scatterings in the Born limit and in the unitary limit. These results are helpful to detect detailed characters of local electronic structures in the vortex lattice states via site-selective NMR experiments.

DOI: 10.1103/PhysRevB.91.014509 PACS number(s): 74.25.Uv, 74.20.Rp, 74.25.nj, 74.25.Ha

I. INTRODUCTION

In the vortex states of type-II superconductors, a kind of Andreev bound state is formed around the vortex core. The bound state has informative structures in the spatial and the energy dependencies, which are different from simple normal states. The structures of the bound state are sensitive to properties of superconductors, such as the pairing symmetry, Fermi surface anisotropy, and multiband superconductivity. Therefore, we can know these properties by the observation of physical quantities reflecting the local electronic structures in the vortex states. Among many experimental methods for the purpose, scanning tunneling microscopy (STM) is a powerful methods to directly observe the local electronic structure [1–3]. However, STM is a method sensitive to the surface condition, and the number of observable materials is restricted.

On the other hand, site-selective NMR experiment is also a method to observe the local electronic structures in the vortex states [4–7]. Since the NMR observation is free from the surface condition, it can be a complementary method to the STM observation. The method of the site-selective NMR is as follows. In the vortex lattice, the internal magnetic field $B(\mathbf{r})$ has spatial variation as shown in the inset of Fig. 1. And the resonance line shape of the NMR given by $P(B) = \int \delta(B - B(\mathbf{r}))d\mathbf{r}$ becomes the broad one called the Redfield pattern. As presented in Fig. 1, among the resonance line shape, the signal from the higher (lower) field comes from the inside (outside) of the vortex core. The signal at the peak of the resonance line shape is from the saddle-point position of the internal fields, i.e., midpoint $r = 0.5a_x$ between nearest-neighbor (NN) vortices. Thus, we can observe the information of local nuclear spin relaxation rate $T_1^{-1}(\mathbf{r})$, tuning the frequency among the resonance line shape. Usually T_1^{-1} is measured only at the peak of the resonance line shape. However, if the observation of T_1^{-1} is performed at different frequencies within the resonance line shape, we can extract rich information about the local electronic states in the vortex states. Thus, the site-selective NMR is expected to play an important role in the study of exotic superconductors through the vortex state properties. In order to establish analysis methods by the site-selective NMR, we need to perform quantitative theoretical calculations for the quantities corresponding to the observation.

*ktanaka@mp.okayama-u.ac.jp
†ichioka@cc.okayama-u.ac.jp

In the uniform states without vortices, it is known that the low-temperature behaviors of T_1^{-1} reflect the energy dependence of the density of states (DOS), $N(E)$, for low-energy excited states within the superconducting gap [8]. For example, in full-gap s-wave superconductors, T_1^{-1} has exponential T dependence at low T since $N(E) = 0$; i.e., low-energy states do not exist within the gap. On the other hand, in the $d_{x^2-y^2}$-wave superconductors with line nodes of the pairing function, T_1^{-1} has power-law dependence $\propto T^3$, since $N(E) \propto E$. When $N(E = 0)$ is finite in the presence of the impurity scatterings, $T_1^{-1} \propto T$. At higher T below the superconducting transition temperature T_c, the T dependence of T_1^{-1} reflects the anisotropy of the pairing function on the Fermi surface. In the s-wave pairing, T_1^{-1} shows a large Hebel-Slichter peak below T_c [9]. On the other hand, the Hebel-Slichter peak is absent in the d-wave pairing. Therefore, the T dependencies of T_1^{-1} is an important method to determine the pairing symmetry of new superconductors. However, usually the NMR observation in a superconductor is performed under the vortex state. We have to be careful to the fact that the behaviors of T_1^{-1} may be different from those of the uniform state. Further, the spatial dependence can be detected by the site-selective NMR. Thus, it is expected that we correctly estimate the behaviors of $T_1^{-1}(\mathbf{r})$, considering the contribution of the vortices.

As for previous theoretical works on the site-selective NMR, the T dependence of $T_1^{-1}(\mathbf{r})$ was calculated in the vortex lattice state by the Bogoliubov–de Gennes theory on the tight-binding atomic lattice model [10]. This calculation was performed near the quantum limit for vortex bound states, and studied only the clean limit, neglecting impurity scatterings. In the quantum limit $\Delta \sim E_F$ (E_F is the Fermi energy and Δ is the superconducting gap), the discretized energy levels of the vortex bound state become eminent. However, most of superconductors in solid states are far from the quantum limit, and within a condition $\Delta \ll E_F$, where the quasiclassical Eilenberger theory can be safely applicable [11]. By the Eilenberger theory, calculations of $T_1^{-1}(\mathbf{r})$ were done for the single vortex case in the chiral p-wave superconductors [12]. Since the quantitative calculation in the whole field range $H_{c1} < H < H_{c2}$ in the vortex lattice state were performed by the Eilenberger theory [13–17], the quantitative estimate of T_1^{-1} is also expected by the calculation in the vortex lattice state, including the H dependence.

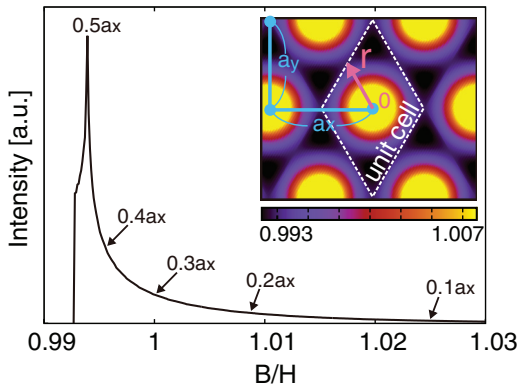

FIG. 1. (Color online) A figure to explain site-selective NMR. The Redfield pattern of the resonance line shape of the NMR, $P(B)$, in the clean limit for the s-wave pairing. $H = 0.02B_0$, $T = 0.1T_c$. This comes from the internal field distribution $B(\mathbf{r})$ presented in the inset. In the inset, dashed line indicates a unit cell of the vortex lattice in our calculations. Arrow indicates radius r ($0 \leqslant r \leqslant 0.5a_x$) from the vortex center along the NN vortex direction, where we study the spatial dependence of T_1^{-1} in Fig. 2. B at each position $r/a_x = 0.1, \ldots, 0.5$ is pointed in the main panel of $P(B)$. a_x is the intervortex distance, and a_y is equal to $\sqrt{3}/2a_x$.

The purpose of this work is to quantitatively estimate the local relaxation rate $T_1^{-1}(\mathbf{r})$ in the vortex lattice state, using the Eilenberger theory and the linear response theory. The T and H dependencies of $T_1^{-1}(\mathbf{r})$ are examined mainly at two typical positions: at the vortex center, and at the midpoint between NN vortices. The latter position represents the outside of the vortex core. We also study influences of nonmagnetic impurity scattering in the Born limit and in the unitary limit. As for the H dependence, we compare results of $(T_1T)^{-1}$ in this work with those of the Knight shift studied in a previous work [17] in order to study the local Korringa relation. In these behaviors of $T_1^{-1}(\mathbf{r})$, we study characteristic natures depending on the pairing symmetry, as we study two pairing cases of the s wave and the $d_{x^2-y^2}$ wave.

This paper is organized as follows. After the introduction, we explain our formulation of Eilenberger theory for the vortex state, and calculation method for T_1^{-1} in Sec. II. In Sec. III, we study the spatial dependence of $T_1^{-1}(\mathbf{r})$, and influences of the nonmagnetic impurity scatterings on the T dependence of $T_1^{-1}(\mathbf{r})$ in the vortex lattice states. In Sec. IV, we discuss the H dependence of $T_1^{-1}(\mathbf{r})$, and make comparison with that of the Knight shift, in the relation to the zero-energy DOS. The last section is devoted to summary.

II. FORMULATION

A. Self-consistent Eilenberger theory

We calculate the spatial structure of vortices in the vortex lattice state by quasiclassical Eilenberger theory, including impurity scatterings [15–17]. We use the quasiclassical Eilenberger theory, where the variation of the atomic scale is integrated out in order to focus on the spatial structure in the order of the superconducting coherence length ξ. For simplicity, we consider the spin-singlet pairing on the two-dimensional cylindrical Fermi surface, $\mathbf{k} = (k_x,k_y) = k_{\rm F}(\cos\theta_k, \sin\theta_k)$, and the Fermi velocity $\mathbf{v}_{\rm F} = v_{\rm F0}\mathbf{k}/k_{\rm F}$. To obtain quasiclassical Green's functions $g(i\omega_n,\mathbf{k},\mathbf{r})$, $f(i\omega_n,\mathbf{k},\mathbf{r})$, $f^\dagger(i\omega_n,\mathbf{k},\mathbf{r})$ in the vortex lattice state, we solve the Riccati equation derived from the Eilenberger equation:

$$\begin{aligned}
&\left\{\omega_n + i\mu B(\mathbf{r}) + \frac{1}{\tau}\langle g\rangle_{\mathbf{k}} + \mathbf{v}\cdot[\nabla + i\mathbf{A}(\mathbf{r})]\right\} f \\
&\quad = \left(\tilde{\Delta}(\mathbf{r},\mathbf{k}) + \frac{1}{\tau}\langle f\rangle_{\mathbf{k}}\right) g, \\
&\left\{\omega_n + i\mu B(\mathbf{r}) + \frac{1}{\tau}\langle g\rangle_{\mathbf{k}} - \mathbf{v}\cdot[\nabla - i\mathbf{A}(\mathbf{r})]\right\} f^\dagger \\
&\quad = \left(\tilde{\Delta}^*(\mathbf{r},\mathbf{k}) + \frac{1}{\tau}\langle f^\dagger\rangle_{\mathbf{k}}\right) g,
\end{aligned} \tag{1}$$

where $g = (1 - ff^\dagger)^{1/2}$, $\mu = \mu_{\rm B}B_0/\pi k_{\rm B}T_{\rm c}$, and $\mathbf{v} = \mathbf{v}_{\rm F}/v_{\rm F0}$. $\langle\cdots\rangle_{\mathbf{k}}$ indicates the Fermi surface average. $\mu_{\rm B}$ is a renormalized Bohr magneton for the Zeeman energy. The order parameter is $\tilde{\Delta}(\mathbf{r},\mathbf{k}) = \Delta(\mathbf{r})\phi(\mathbf{k})$ with the pairing function $\phi(\mathbf{k}) = \sqrt{2}(k_x^2 - k_y^2)/k_{\rm F}^2$ for the $d_{x^2-y^2}$-wave pairing, or $\phi(\mathbf{k}) = 1$ for the s-wave pairing. $\mathbf{r}$ is the center-of-mass coordinate of the pair. In our calculations, length, temperature, and magnetic field are, respectively, measured in units of ξ_0, $T_{\rm c}$, and B_0. Here, $\xi_0 = \hbar v_{\rm F0}/2\pi k_{\rm B}T_{\rm c}$, and $B_0 = \phi_0/2\pi\xi_0^2$ with the flux quantum ϕ_0. $T_{\rm c}$ is the superconducting transition temperature in the clean limit at a zero magnetic field. The energy E, pair potential Δ, and Matsubara frequency ω_n are in units of $\pi k_{\rm B}T_{\rm c}$. In the following, we set $\hbar = k_{\rm B} = 1$.

As magnetic fields are applied to the z axis, the vector potential is given by $\mathbf{A}(\mathbf{r}) = \frac{1}{2}\mathbf{H}\times\mathbf{r} + \mathbf{a}(\mathbf{r})$ in the symmetric gauge, where $\mathbf{H} = (0,0,H)$ is a uniform flux density, and $\mathbf{a}(\mathbf{r})$ is related to the internal field $\mathbf{B}(\mathbf{r}) = (0,0,B(\mathbf{r})) = \mathbf{H} + \nabla\times\mathbf{a}(\mathbf{r})$. As shown in the inset of Fig. 1, the unit cell of the vortex lattice is given by $\mathbf{r} = s_1(\mathbf{u}_1 - \mathbf{u}_2) + s_2\mathbf{u}_2$ with $-0.5 \leqslant s_i \leqslant 0.5$ ($i = 1,2$), $\mathbf{u}_1 = (a_x,0,0)$, $\mathbf{u}_2 = (a_x/2,a_y,0)$, and $a_xa_yH = \phi_0$. $a_y/a_x = \sqrt{3}/2$ for the triangular vortex lattice.

Impurity scattering is treated by the t-matrix approximation [15,17–23], assuming s-wave nonmagnetic impurity scattering. Thus, $1/\tau$ in Eq. (1) is given by

$$\frac{1}{\tau} = \frac{1/\tau_0}{\cos^2\delta_0 + \left(\langle g\rangle_{\mathbf{k}}^2 + \langle f\rangle_{\mathbf{k}}\langle f^\dagger\rangle_{\mathbf{k}}\right)\sin^2\delta_0}, \tag{2}$$

where $\delta_0 = \tan^{-1}(\pi N_0u_0)$, and u_0 is the potential of impurity strength. N_0 is the DOS at the Fermi energy in the normal state. τ_0 is a scattering time of the normal state, and given by $1/\tau_0 = n_{\rm s}N_0u_0^2/(1 + \pi^2N_0^2u_0^2)$, where $n_{\rm s}$ is the number density of impurities. In this paper, we use a unit of time as $\hbar/2\pi k_BT_{\rm c}\tau_0 \to 1/\tau_0$. We consider two limits of the impurity scatterings; i.e., $\delta_0 \to 0$ in the Born limit, and $\delta_0 \to \pi/2$ in the unitary limit.

To determine the pair potential $\Delta(\mathbf{r})$ and the quasiclassical Green's functions self-consistently, we calculate $\Delta(\mathbf{r})$ by the gap equation

$$\Delta(\mathbf{r}) = g_0N_0T\sum_{0<\omega_n\leqslant\omega_{\rm cut}}\langle\phi^*(\mathbf{k})(f + f^{\dagger *})\rangle_{\mathbf{k}}, \tag{3}$$

where $(g_0N_0)^{-1} = \ln T + 2T\sum_{0<\omega_n\leqslant\omega_{\rm cut}}\omega_n^{-1}$, and we use $\omega_{\rm cut} = 20k_{\rm B}T_{\rm c}$. For the self-consistent calculation of the vector

potential for the internal field $B(\mathbf{r})$, we use the relation

$$\nabla \times (\nabla \times \mathbf{A}) = \nabla \times \mathbf{M}_{\rm para}(\mathbf{r}) - \frac{2T}{\kappa^2} \sum_{0<\omega_n} \langle \mathbf{v} {\rm Im}\{g\} \rangle_{\mathbf{k}}, \quad (4)$$

where the paramagnetic moment $\mathbf{M}_{\rm para}(\mathbf{r}) = (0,0,M_{\rm para}(\mathbf{r}))$ and

$$M_{\rm para}(\mathbf{r}) = M_0 \left(\frac{B(\mathbf{r})}{H} - \frac{2T}{\mu H} \sum_{0<\omega_n} \langle {\rm Im}\{g\} \rangle_{\mathbf{k}} \right) \quad (5)$$

with the paramagnetic moment in the normal state, $M_0 = (\mu/\kappa)^2 H$. The Ginzburg-Landau parameter is given by $\kappa = B_0/\pi k_{\rm B} T_{\rm c} \sqrt{8\pi N_0}$. In our calculations, we use $\kappa = 30$ as a typical type-II superconductor. As for the paramagnetic effect, we use $\mu = 0.01$ in order to estimate the paramagnetic moment induced by the applied magnetic field. In this small μ, the effects of the paramagnetic pair-breaking are negligible [16].

We iterate calculations of Eqs. (1)–(5) in Matsubara frequency ω_n until we obtain the self-consistent results of $\mathbf{A}(\mathbf{r})$, $\Delta(\mathbf{r})$, and the quasiclassical Green's functions. Thus, we determine the spatial structure of $\mathbf{A}(\mathbf{r})$ and $\Delta(\mathbf{r})$ in the vortex lattice state.

B. Nuclear relaxation rate

Next, using the self-consistently obtained $\mathbf{A}(\mathbf{r})$ and $\Delta(\mathbf{r})$, we calculate the quasiclassical Green's functions and the self-energies in real energy $E \pm i\eta$ instead of $i\omega_n$. We solve Eilenberger equation (1) with $i\omega_n \to E \pm i\eta$ to obtain $g(E \pm i\eta,\mathbf{k},\mathbf{r})$, $f(E \pm i\eta,\mathbf{k},\mathbf{r})$, $f^\dagger(E \pm i\eta,\mathbf{k},\mathbf{r})$. η is a small parameter, and we use $\eta = 0.01$ in our numerical calculation. From the quasiclassical Green's functions, we obtain the self-energy $\frac{1}{\tau}\langle g \rangle_{\mathbf{k}}$, $\frac{1}{\tau}\langle f \rangle_{\mathbf{k}}$, $\frac{1}{\tau}\langle f^\dagger \rangle_{\mathbf{k}}$ in the real energy. These calculations are iterated until we obtain self-consistent results for the quasi-classical Green's functions in real E. The local DOS $N(E,\mathbf{r})$ is given by $N(E,\mathbf{r}) = \langle {\rm Re}\{g(E + i\eta,\mathbf{k},\mathbf{r})\} \rangle_{\mathbf{k}}$.

The equation to estimate the nuclear relaxation rate T_1^{-1} is derived by the linear response theory [12,24], and given by

$$\frac{[T_1(T)T]^{-1}}{[T_1(\tilde{T}_{\rm c})\tilde{T}_{\rm c}]^{-1}} = \frac{[T_{1gg}(T)T]^{-1} + [T_{1ff}(T)T]^{-1}}{[T_1(\tilde{T}_{\rm c})\tilde{T}_{\rm c}]^{-1}} = \int_{-\infty}^{\infty} \frac{W_{gg}(E,\mathbf{r}) + W_{ff}(E,\mathbf{r})}{4T\cosh^2(E/2T)} dE, \quad (6)$$

where

$$W_{gg}(E,\mathbf{r}) = \langle a^{22}_{\downarrow\downarrow}(E,\mathbf{k},\mathbf{r}) \rangle_{\mathbf{k}} \langle a^{11}_{\uparrow\uparrow}(-E,\mathbf{k},\mathbf{r}) \rangle_{\mathbf{k}},$$
$$W_{ff}(E,\mathbf{r}) = -\langle a^{21}_{\downarrow\uparrow}(E,\mathbf{k},\mathbf{r}) \rangle_{\mathbf{k}} \langle a^{12}_{\uparrow\downarrow}(-E,\mathbf{k},\mathbf{r}) \rangle_{\mathbf{k}}, \quad (7)$$

with

$$a^{11}_{\uparrow\uparrow}(E,\mathbf{k},\mathbf{r}) = \frac{1}{2\pi}[g(E + i\eta,\mathbf{k},\mathbf{r}) - g(E - i\eta,\mathbf{k},\mathbf{r})],$$
$$a^{22}_{\downarrow\downarrow}(E,\mathbf{k},\mathbf{r}) = \frac{1}{2\pi}[\bar{g}(E + i\eta,\mathbf{k},\mathbf{r}) - \bar{g}(E - i\eta,\mathbf{k},\mathbf{r})],$$
$$a^{12}_{\uparrow\downarrow}(E,\mathbf{k},\mathbf{r}) = \frac{i}{2\pi}[f(E + i\eta,\mathbf{k},\mathbf{r}) - f(E - i\eta,\mathbf{k},\mathbf{r})],$$
$$a^{21}_{\downarrow\uparrow}(E,\mathbf{k},\mathbf{r}) = \frac{i}{2\pi}[f^\dagger(E + i\eta,\mathbf{k},\mathbf{r}) - f^\dagger(E - i\eta,\mathbf{k},\mathbf{r})], \quad (8)$$

and $\bar{g}(E,\mathbf{k},\mathbf{r}) = g(-E,\mathbf{k},\mathbf{r})$, $\tilde{T}_{\rm c}(<T_c)$ is superconducting transition temperature at a finite magnetic field, while T_c is transition temperature at a zero field in the clean limit. $(T_{1gg}T)^{-1}$ is the contribution in $(T_1T)^{-1}$ from the term W_{gg}, and $(T_{1ff}T)^{-1}$ is the contribution from the coherence term W_{ff}. Substituting self-consistently obtained quasiclassical Green's functions to Eq. (8), we numerically calculate local $(T_1T)^{-1}$.

III. T DEPENDENCE

A. s-wave pairing

First, we study the T dependence of the local nuclear relaxation rate T_1^{-1} in the clean limit. We present T_1^{-1} as a function of T at some positions on a line between NN vortices for the s-wave pairing in Fig. 2(a). At the midpoint $r = 0.5a_x$ in the s-wave pairing, T_1^{-1} shows exponential-like T dependence at low T, and has a Hebel-Slichter peak below $\tilde{T}_{\rm c}$. There are similar behaviors to those at a zero field. Approaching the vortex center with decreasing r, the Hebel-Slichter peak is smeared. Further approaching the vortex core, we see the enhancement in the middle T region. While this enhancement resembles the Hebel-Slichter peak at $r = 0.5a_x$, the origin is different. The Hebel-Slichter peak mainly comes from the enhancement of the coherence term T_{1ff}^{-1}. However, the peak

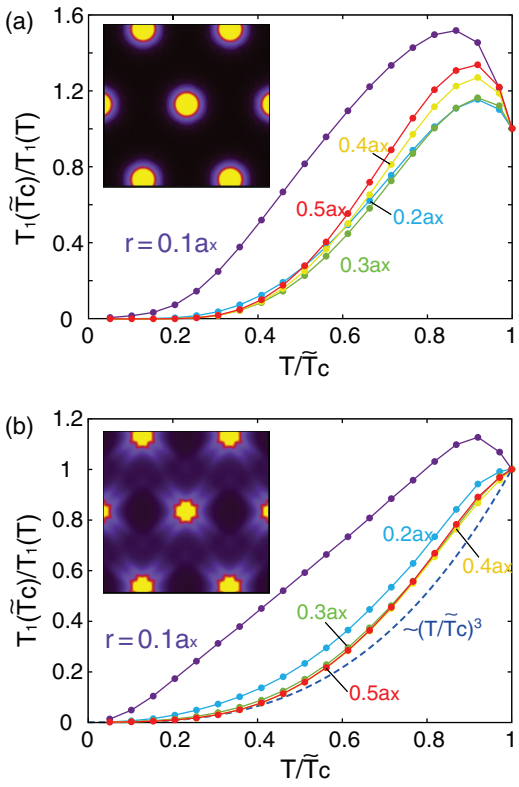

FIG. 2. (Color online) (a) Spatial variation of local T_1^{-1} for the s-wave pairing in the clean limit. We show the T dependence of $T_1^{-1}(T)/T_1^{-1}(\tilde{T}_{\rm c})$ at radius $r/a_x = 0.1, \ldots, 0.5$ from the vortex center along the NN direction in Fig. 1. $H = 0.02B_0$ and $T = 0.1T_{\rm c}$. The inset shows a density plot of the spatial structure of local T_1^{-1} in the clean limit for the s-wave pairing. (b) The same as (a), but for the $d_{x^2-y^2}$-wave pairing. We also show a dashed line for $(T/\tilde{T}_{\rm c})^3$.

at $r = 0.1a_x$ appears by the enhancement of T_{1gg}^{-1} without contributions of T_{1ff}^{-1}. At the vortex core, T_{1gg}^{-1} becomes larger at lower T than T_c, because larger DOS appears at lower energies within the superconducting gap. With approaching the vortex center, the peak temperature of T_1^{-1} is shifted to lower T, since the peak energy of the low-energy DOS decreases, approaching the zero energy at the center. The inset in Fig. 2 presents the spatial structure of T_1^{-1} at low T. There we see that T_1^{-1} is largely enhanced inside the vortex core, reflecting low-energy excitations due to the vortex bound states. Thus, we can extract the information of the vortex bound state through the spatial-dependence of T_1^{-1} by tuning the resonance frequency as in Fig. 1 in the site-selective NMR measurement.

To see the influences of the magnetic field at the position outside of the core, in Fig. 3(a) we present the T dependence of $(T_1T)^{-1}$ at the midpoint $r = 0.5a_x$. The midpoint $r = 0.5a_x$ is a significant position because the frequency of the internal field at the midpoint corresponds to the peak frequency of the Redfield pattern in Fig. 1. There, for $H \to 0$, T_1^{-1} has exponential T dependence at low T. In the presence of low H, $(T_1T)^{-1}$ is not largely changed at low T in the scale of vertical axis in Fig. 3(a). At higher T there appears a Hebel-Slichter peak below $\tilde{T}_c$ at low H. With raising H, we see the suppression of the Hebel-Slichter peak. At high $H = 0.42B_0$ in Fig. 3(a), on lowering T, $(T_1T)^{-1}$ monotonically decreases without the Hebel-Slichter peak. The suppression of the Hebel-Slichter peak by increasing magnetic fields was observed in NMR experiments [25–27]. In Fig. 3(b), a line presents the H dependence of the Hebel-Slichter peak's height in the clean limit. With increasing H, the peak height rapidly decreases, and the height is 1.2 times the normal-state value at $H = 0.1H_{c2}$.

To discuss the reason of the suppression for the Hebel-Slichter peak, in Figs. 3(c) and 3(d) we present $(T_{1gg}T)^{-1}$ and $(T_{1ff}T)^{-1}$, respectively. These are decompositions of $(T_1T)^{-1}$ to the contributions of W_{gg} and W_{ff} in Eq. (7). In the T dependence of $(T_{1gg}T)^{-1}$, the small peak below $\tilde{T}_c$ at $H = 0$ is due to a peak at the gap edge in the DOS. With increasing H, $(T_{1gg}T)^{-1}$ below $\tilde{T}_c$ is suppressed. The main contribution to the Hebel-Slichter peak comes from the coherence term $(T_{1ff}T)^{-1}$ in Fig. 3(d). This contribution is also decreased by an increase of H. The decrease of $(T_{1gg}T)^{-1}$ and $(T_{1ff}T)^{-1}$ below $\tilde{T}_c$ is related to the smearing of the gap edge in the DOS, as shown in Fig. 3(e). There, we see that the gap edge in the local DOS is gradually smeared with increasing H. The smearing is eminent even at low fields, while the local zero-energy DOS is still small there. The zero-energy DOS at midpoint comes from a small tail of the vortex bound state penetrating from the vortex core.

In the s-wave pairing, behaviors of T_1^{-1} are not seriously affected by the impurity scatterings at the midpoint, suggesting a remnant of the Anderson theorem [28] for the nonmagnetic impurity scattering at $H = 0$. Thus, the Hebel-Slichter peak appears as in the clean limit. Square points in Fig. 3(b) show the H dependence of the peak height in the presence of impurity scatterings in the Born limit. There, we see similar H dependencies to those in the clean limit. The peak height in the unitary limit also shows similar behavior (not shown in the figure).

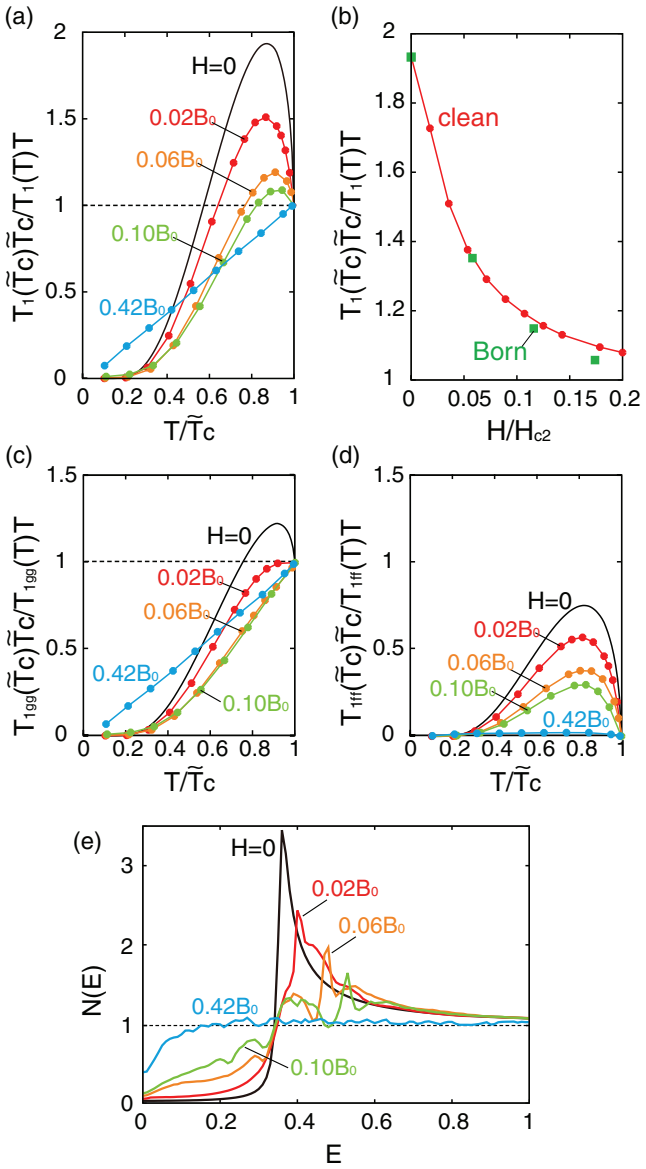

FIG. 3. (Color online) (a) T dependence of $(T_1T)^{-1}$ at the midpoint $r = 0.5a_x$ for the s-wave pairing in the clean limit, where $H_{c2} = 0.56B_0$ at $T = 0.1T_c$. We plot renormalized value $[T_1(T)T]^{-1}/[T_1(\tilde{T}_c)\tilde{T}_c]^{-1}$ at $H/B_0 = 0$, 0.02, 0.06, 0.10, 0.42. (b) Height of the Hebel-Slichter peak as a function of H/H_{c2}. We plot maximum value of $[T_1(T)T]^{-1}/[T_1(\tilde{T}_c)\tilde{T}_c]^{-1}$. Solid line indicates the case of the clean limit. Square points are for the Born limit with $1/\tau_0 = 0.2$, where $H_{c2} = 0.69B_0$ at $T = 0.1T_c$. (c) T dependence of the contribution $(T_{1gg}T)^{-1}$ from the W_{gg} term among $(T_1T)^{-1}$ in (a). (d) T dependence of the contribution $(T_{1ff}T)^{-1}$ from the coherence term W_{gg}. (e) Local DOS $N(E,\mathbf{r})$ at the midpoint at $H/B_0 = 0$, 0.02, 0.06, 0.10, 0.42 in the s-wave pairing. $T = 0.85\tilde{T}_c$.

B. $d_{x^2-y^2}$-wave pairing

In Fig. 2(b), we present T_1^{-1} as a function of T at some positions for the $d_{x^2-y^2}$-wave pairing in the clean limit. The behaviors at $r/a_x = 0.3$, 0.4, 0.5 outside of the vortex core are similar to those at $H = 0$. At low T range, $T_1^{-1} \propto T^3$ at a zero field as shown by the dashed line in the Fig. 2(b). A difference from the s-wave pairing is the existence of nodes

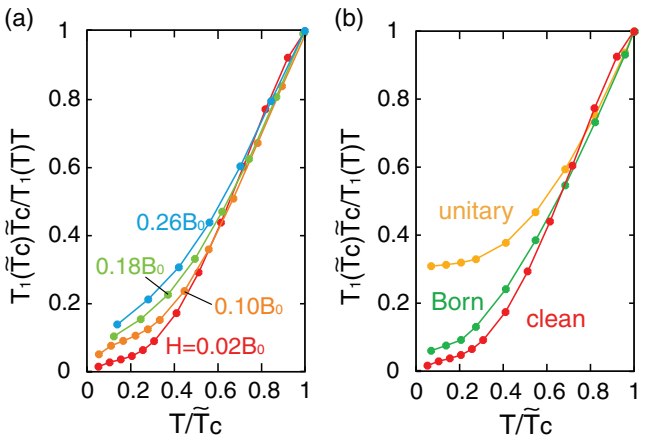

FIG. 4. (Color online) T dependence of $(T_1T)^{-1}$ for the $d_{x^2-y^2}$-wave pairing at the midpoint $r = 0.5a_x$ between NN vortices. (a) We plot $[T_1(T)T]^{-1}/[T_1(\tilde{T}_c)\tilde{T}_c]^{-1}$ at $H/B_0 = 0.02$, 0.10, 0.18, 0.26 in the clean limit, where $H_{c2} = 0.60B_0$ at $T = 0.1T_c$. (b) T dependence of $[T_1(T)T]^{-1}/[T_1(\tilde{T}_c)\tilde{T}_c]^{-1}$ at $H = 0.02B_0$ in the Born limit and the unitary limit with $1/\tau_0 = 0.1$. We also plot $(T_1T)^{-1}$ in the clean limit for comparison.

in the d-wave pairing function $\phi(\mathbf{k})$, where the sign of $\phi(\mathbf{k})$ changes along the Fermi surface. Since anomalous Green's functions have the same sign change as in $\phi(\mathbf{k})$, the Fermi surface average $\langle f\rangle_{\mathbf{k}} = \langle f^\dagger\rangle_{\mathbf{k}} = 0$ so that the coherence term $W_{ff} = 0$ and the Hebel-Slichter peak vanishes. At low T, T_1^{-1} shows power-law behavior due to the line nodes in the d-wave pairing.

Near the vortex core $r = 0.1a_x$ in Fig. 2(b), we see the enhancement of T_1^{-1}, reflecting low-energy excitations of the vortex bound states as in the s-wave pairing. The spatial variation of $(T_1T)^{-1}$ at low T is presented in the inset panel of Fig. 2(b). There, the rapid relaxation regions localized around vortex cores have fourfold shape. This reflects the fourfold symmetry of the pairing function and the intervortex interference of low-energy electronic states extending to outside of the vortex core [14]. Due to the fourfold shape of the vortex core, the triangular vortex lattice at low H is deformed to the square vortex lattice at high H. Thus, we perform our calculations also in the square vortex lattice case [17], and confirm that results for the T and H dependence of T_1^{-1} do not seriously depend on the shape of the vortex lattice at the midpoint and the vortex core. Therefore, we present results only for the triangular vortex lattice case in this paper. In Fig. 4(a), we present the T dependence of T_1^{-1} at some H. The low-T behavior of $(T_1T)^{-1} \propto T^2$ at a zero field changes to that $(T_1T)^{-1}$ reduces to a finite value due to the residual DOS under magnetic fields. In the $d_{x^2-y^2}$-wave pairing, low-energy excitations at the vortex core easily extend toward the outside of the core by the node of the pairing function [14]. The residual values of $(T_1T)^{-1}$ at low T increase with H. The increase is visible in Fig. 4(a) even at low H in the d-wave pairing, while it is very small in Fig. 3(a) in the s-wave pairing.

To discuss influences of the impurity scatterings in the vortex state for the $d_{x^2-y^2}$-wave pairing, we show the T dependence of $(T_1T)^{-1}$ at the midpoint between NN vortices in Fig. 4(b). There, we plot the T dependence of $(T_1T)^{-1}$ at a low field $H = 0.02B_0$ in the Born limit and the unitary limit in addition to the clean limit. By the impurity scattering, the upper critical field is suppressed to $H_{c2} = 0.35B_0$ from $0.60B_0$ of the clean limit at $T = 0.1T_c$. At low T, the residual values of $(T_1T)^{-1}$ are increased by the impurity scatterings. Particularly in the unitary limit, $(T_1T)^{-1}$ is remarkably increased and $(T_1T)^{-1}$ is reduced to be a constant at the low T range. Actually, this tendency is observed in NMR and NQR experiments [29].

IV. H DEPENDENCE

In this section, we study the H dependence of residual value of $(T_1T)^{-1}$ at low T for the s-wave and the d-wave pairings. In the low temperature limit, $(T_1T)^{-1}$ in Eq. (6) is proportional to square of the zero-energy DOS $N(E = 0)$ in the uniform state. On the other hand, it is known that the Knight shift M of the paramagnetic susceptibility is proportional to $N(E = 0)$. Thus, we expect the Korringa relation $(T_1T)^{-1} \propto M^2$, which is usually considered in the normal states [30,31]. From the Korringa relation,

$$(T_1T)^{-1/2} \sim M \sim N(E = 0), \tag{9}$$

where each quantity is renormalized by the normal-state value. We examine this relation locally in the H dependence in the vortex states.

A. At a midpoint

First we consider the H dependence of $(T_1T)^{-1/2}$ at the midpoint between NN vortices, which is presented by solid lines in Fig. 5 for the clean limit, the Born limit, and the unitary limit. In the clean limit, compared to the $d_{x^2-y^2}$-wave pairing case in Fig. 5(b), $(T_1T)^{-1/2}$ is smaller in the s-wave pairing in Fig. 5(a). There, the slope as a function of H is smaller at low H, and shows rapid increase near H_{c2} in the s-wave pairing.

In the s-wave pairing in Fig. 5(a), the nonmagnetic impurity scatterings do not seriously change $(T_1T)^{-1}$ in the low H range, indicating the remnant of the Anderson theorem [28] in the s-wave superconductor. At higher fields $H > 0.5H_{c2}$, the contributions of the impurity scatterings appear even in the s-wave pairing, and enhance $(T_1T)^{-1}$. On the other hand, in the $d_{x^2-y^2}$-wave pairing, the contributions of the impurity scatterings to enhance $(T_1T)^{-1}$ are eminent in all field ranges from $H = 0$ to H_{c2}. Compared to the Born limit with the same $1/\tau_0$, $(T_1T)^{-1}$ in the unitary limit is larger, and it remains finite even at $H \to 0$.

The above-mentioned behaviors of $(T_1T)^{-1}$ are related to the local DOS and the Knight shift. From the spatial variation of paramagnetic moment $M_{\rm para}(\mathbf{r})$ in Eq. (5), we obtain the distribution $P(M) = \int \delta(M - M_{\rm para}(\mathbf{r}))d\mathbf{r}$. The T and H dependencies of $P(M)$ were reported in Ref. [17]. There, we found that $M_{\rm para}(\mathbf{r})$ is minimum or near minimum at the midpoint in many cases of H and T. Since the minimum of $M_{\rm para}(\mathbf{r})$ corresponds to the minimum edge $M_{\rm min}$ of $P(M)$, we plot the H dependence of $M_{\rm min}$ by the dashed lines in Fig. 5. There, we see that the local Korringa relation in Eq. (9) is roughly satisfied, since the H dependencies of $(T_1T)^{-1}$ and $M_{\rm min}$ show similar behaviors. A typical difference

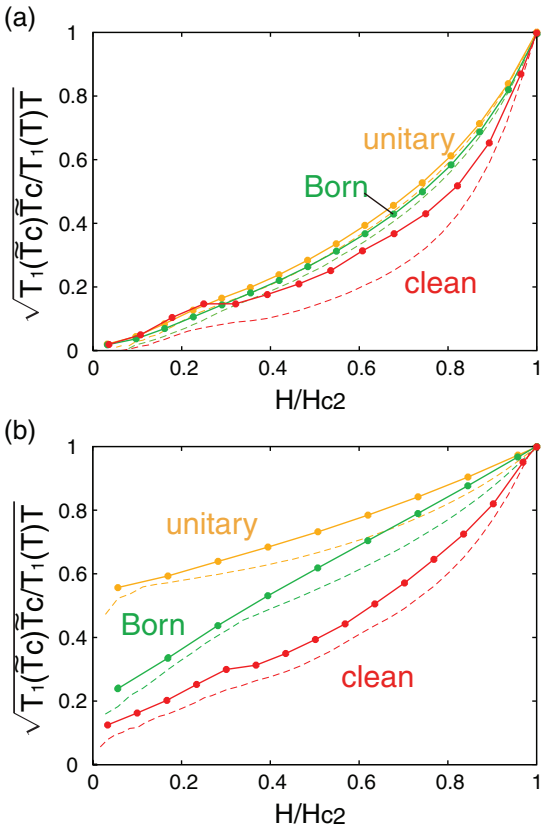

FIG. 5. (Color online) Solid lines indicate the H dependence of $[T_1(T)T]^{-1/2}/[T_1(\tilde{T}_c)\tilde{T}_c]^{-1/2}$ at the midpoint between NN vortices. In addition to the clean limit $1/\tau_0 = 0$, we present the Born limit and the unitary limit of the nonmagnetic impurity scattering with $1/\tau_0 = 0.1$. Dashed lines indicate the minimum of the paramagnetic moment, $M_{\rm min}$, in the vortex lattice state. $T = 0.1T_c$. (a) s-wave pairing. (b) $d_{x^2-y^2}$-wave pairing.

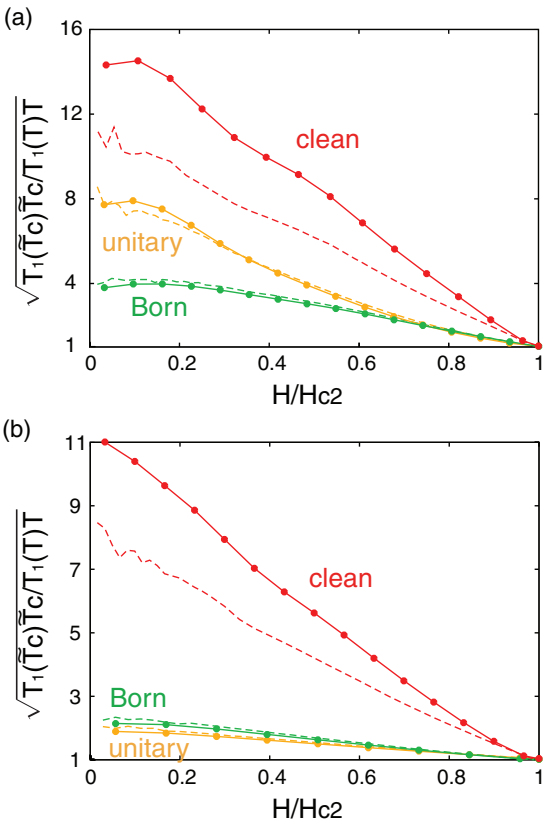

FIG. 6. (Color online) Solid lines indicate the H dependence of $[T_1(T)T]^{-1/2}/[T_1(\tilde{T}_c)\tilde{T}_c]^{-1/2}$ at the vortex center. We present three cases: the clean limit of $1/\tau_0 = 0$, the Born limit, and the unitary limit for the nonmagnetic impurity scattering of $1/\tau_0 = 0.1$. Dashed lines present the paramagnetic moment $M_{\rm max}$ at the vortex center. $T = 0.1T_c$. (a) s-wave pairing. (b) $d_{x^2-y^2}$-wave pairing.

between the s-wave and the d-wave pairing appears in the H dependence of $N(E = 0)$; i.e., $N(E = 0) \propto H$ for the s-wave pairing, and $N(E = 0) \propto H^{1/2}$ for the d-wave pairing at low H range [16,32]. Also in the Knight shift spectrum, the weighted center M_χ of $P(M)$, which is the spatial average of $M_{\rm para}(\mathbf{r})$, follows these relations [17]. However, if the outside of the vortex core is selectively observed such as $M_{\rm min}$, the H dependence is largely deviated from the H or $H^{1/2}$ relations.

B. At a vortex center

Next, we study $(T_1T)^{-1/2}$ at the vortex center. There, T_1^{-1} monotonically increases on lowering T, because of the low-energy quasiparticles confined inside the vortex core. In Fig. 6, we plot $(T_1T)^{-1/2}$ at the vortex center as a function of H/H_{c2} in the clean limit, the Born limit, and the unitary limit. With decreasing H, $(T_1T)^{-1}$ is enhanced at the vortex center. There, enhanced $(T_1T)^{-1/2}$ at low H is about 10 times larger than the normal-state value in the clean limit.

In the s-wave pairing case in Fig. 6(a), the impurity scatterings make $(T_1T)^{-1}$ smaller even at low fields at the vortex center, while the changes by the impurity scatterings are not seen at the midpoint in Fig. 5(a). This indicates that the Anderson theorem [28] is broken at the vortex core even in the s-wave pairing, reflecting the phase winding of the vortex. The Anderson theorem is broken when $\langle f\rangle_{\mathbf{k}}$ is suppressed compared to $\langle g\rangle_{\mathbf{k}}$. In the d-wave pairing, the Anderson theorem is broken, since $\langle f\rangle_{\mathbf{k}} = 0$ due to the sign change of the pairing function $\phi(\mathbf{k})$. In the bulk s-wave superconductor, $\langle f\rangle_{\mathbf{k}}$ is not canceled by the Fermi surface average. However, around the vortex core, the phase factor of f varies depending on $\mathbf{k}$, because the phase factor of $\Delta(\mathbf{r})$ changes along the quasiparticle trajectory of the $\mathbf{k}$ direction. Therefore, $\langle f\rangle_{\mathbf{k}}$ is suppressed by the Fermi surface average, and the Anderson theorem is broken. The suppression by the impurity scatterings is larger in the Born limit, reflecting the difference of low-energy states between the Born limit and the unitary limit at the vortex core [21]. In the $d_{x^2-y^2}$-wave pairing in Fig. 6(b), the weight of suppression by the impurity scatterings is larger, compared to the s-wave pairing. $(T_1T)^{-1}$ in the unitary limit is smaller than that in the Born limit.

For comparison, by the dashed lines in Fig. 6 we also show the H dependence of the paramagnetic moment $M_{\rm para}(\mathbf{r})$ at the vortex core, which is the maximum edge $M_{\rm max}$ of $P(M)$. In the presence of impurity scatterings, we see the local Korringa relation $(T_1T)^{-1/2} \sim M_{\rm max}$ is well satisfied also at the vortex center. On the other hand, in the clean limit we see the deviation of $(T_1T)^{-1/2}$ from $M_{\rm max}$, while they both show similar H

dependence. This is because the spectrum of $N(E)$ has a sharp peak near $E = 0$ in the clean limit. When $N(E)$ has rapid E dependence near $E = 0$, the local Korringa relation is not necessarily satisfied, since the dependence of the integrand on $N(E)$ is different in the equations for $(T_1T)^{-1}$ and for M.

V. SUMMARY AND DISCUSSION

On the basis of Eilenberger theory, we performed a quantitative estimate of the local NMR relaxation rate T_1^{-1} in the vortex lattice state, focusing on the difference between the s-wave and the $d_{x^2-y^2}$-wave pairing symmetries. We studied the T and H dependence of $(T_1T)^{-1}$ in the spatial variation of the vortex lattice, to know the characteristic behaviors at the vortex core and outside of the core. For example, we showed how the Hebel-Sclichter peak of $(T_1T)^{-1}$ in the s-wave pairing is smeared by applying magnetic fields. We also investigated influences of the nonmagnetic impurity scatterings both in the Born limit and in the unitary limit. In the s-wave pairing, effects of the nonmagnetic impurity scatterings are very weak outside of the core, but the effects work well inside the vortex core at low fields. On the other hand, $(T_1T)^{-1}$ in the $d_{x^2-y^2}$-wave pairing is affected by the nonmagnetic impurity scatterings both outside and inside the vortex core, where the impurity effect is larger in the unitary limit than in the Born limit. At low T, we compared the H dependence of $(T_1T)^{-1}$ and the Knight shift of the paramagnetic moment to examine the local Korringa relation. These H dependencies come from the local electronic states reflecting the pairing symmetry.

The electronic structures in the vortex states were studied by the Eilenberger theory also in multiband [33] and anisotropic s-wave [34] superconductors. The site-selective NMR in these superconductors is one of interesting topics, and belongs to future works. In the multiband superconductor, zero-energy DOS $N(E = 0)$ as a function of H rapidly increases at low H by the contributions of a band with small superconducting gap [33]. In the anisotropic s-wave superconductors, the H dependence of $N(E = 0)$ shows intermediate behavior between isotropic s-wave and nodal d-wave superconductors [34]. As suggestions from results in this paper, T_{1gg}^{-1} in the site-selective NMR will follow the characteristic H dependence of local $N(E = 0)$ also in multiband and anisotropic s-wave superconductors. We note that the anisotropic s-wave gap without the sign change is effectively changed to the isotropic gap by the nonmagnetic impurity scatterings. This is reflected in T_{1ff}^{-1} near T_c. Actually, the Hebel-Slichter peak is enhanced in anisotropic s-wave superconductors by the nonmagnetic impurity effect smearing the gap anisotropy [35].

These results are helpful to analyze the results of the site-selective NMR in order to study the local electronic structure in the vortex state through the T and the H dependence and the spatial variations.

ACKNOWLEDGMENTS

This work was supported by Grants-in-Aid for Scientific Research No. 26400360 and No. 25103716 from the Japan Society for the Promotion of Science.

[1] H. F. Hess, R. B. Robinson, and J. V. Waszczak, Phys. Rev. Lett. **64**, 2711 (1990).
[2] N. Nakai, P. Miranović, M. Ichioka, H. F. Hess, K. Uchiyama, H. Nishimori, S. Kaneko, N. Nishida, and K. Machida, Phys. Rev. Lett. **97**, 147001 (2006).
[3] S. Kaneko, K. Matsuba, M. Hafiz, K. Yamasaki, E. Kakizaki, N. Nishida, H. Takeya, K. Hirata, T. Kawakami, T. Mizushima, and K. Machida, J. Phys. Soc. Jpn. **81**, 063701 (2012).
[4] N. J. Curro, C. Milling, J. Haase, and C. P. Slichter, Phys. Rev. B **62**, 3473 (2000).
[5] V. F. Mitrović, E. E. Sigmund, M. Eschrig, H. N. Bachman, W. P. Halperin, A. P. Reyes, P. Kuhns, and W. G. Moulton, Nature (London) **413**, 501 (2001).
[6] K. Kakuyanagi, K.-ichi Kumagai, and Y. Matsuda, Phys. Rev. B **65**, 060503(R) (2002); K. Kakuyanagi, K. Kumagai, Y. Matsuda, and M. Hasegawa, Phys. Rev. Lett. **90**, 197003 (2003).
[7] Y. Nakai, Y. Hayashi, K. Kitagawa, K. Ishida, H. Sugawara, D. Kikuchi, and H. Sato, J. Phys. Soc. Jpn. **77**, 333 (2008); Y. Nakai, Y. Hayashi, K. Ishida, H. Sugawara, D. Kikuchi, and H. Sato, Physica B **403**, 1109 (2008).
[8] M. Sigrist and K. Ueda, Rev. Mod. Phys. **63**, 239 (1991).
[9] L. C. Hebel and C. P. Slichter, Phys. Rev. **113**, 1504 (1959).
[10] M. Takigawa, M. Ichioka, and K. Machida, Phys. Rev. Lett. **83**, 3057 (1999); J. Phys. Soc. Jpn. **69**, 3943 (2000).
[11] G. Eilenberger, Z. Phys. **214**, 195 (1968).
[12] N. Hayashi and Y. Kato, Physica C **388-389**, 513 (2003); J. Low Temp. Phys. **131**, 893 (2003).
[13] U. Klein, J. Low Temp. Phys. **69**, 1 (1987).
[14] M. Ichioka, A. Hasegawa, and K. Machida, Phys. Rev. B **59**, 184 (1999); **59**, 8902 (1999).
[15] P. Miranović, M. Ichioka, and K. Machida, Phys. Rev. B **70**, 104510 (2004).
[16] M. Ichioka and K. Machida, Phys. Rev. B **76**, 064502 (2007); M. Ichioka, K. M. Suzuki, Y. Tsutsumi, and K. Machida, in *Superconductivity—Theory and Applications*, edited by A. M. Luiz (InTech, Croatia, 2011), Chap. 10.
[17] K. K. Tanaka, M. Ichioka, N. Nakai, and K. Machida, Phys. Rev. B **89**, 174504 (2014).
[18] E. V. Thuneberg, J. Kurkijärvi, and D. Rainer, Phys. Rev. B **29**, 3913 (1984).
[19] Y. Kato, J. Phys. Soc. Jpn. **69**, 3378 (2000).
[20] N. Hayashi and Y. Kato, Phys. Rev. B **66**, 132511 (2002).
[21] M. Eschrig, D. Rainer, and J. A. Sauls, in *Vortices in Unconventional Superconductors and Superfluids*, edited by R. P. Huebener, N. Schopohl, and G. E. Volovik (Springer, Heidelberg, 2002), p. 175; Vortex core structure and dynamics in layered superconductors, arXiv:cond-mat/0106546.
[22] N. Hayashi, Y. Kato, and M. Sigrist, J. Low Temp. Phys. **139**, 79 (2005).
[23] J. A. Sauls and M. Eschrig, New J. Phys. **11**, 075008 (2009).
[24] Y. Nagai, N. Hayashi, N. Nakai, H. Nakamura, M. Okumura, and M. Machida, New J. Phys. **10**, 103026 (2008).
[25] B. G. Silbernagel, M. Wegner, and J. E. Wernick, Phys. Rev. Lett. **17**, 384 (1966).

[26] Y. Masuda and N. Okubo, J. Phys. Soc. Jpn. **26**, 309 (1969).
[27] Y. Nakai, K. Ishida, D. Kikuchi, H. Sugawara, and H. Sato, J. Phys. Soc. Jpn. **74**, 3370 (2005).
[28] P. W. Anderson, J. Phys. Chem. Sol. **11**, 26 (1959).
[29] K. Ishida, Y. Kitaoka, N. Ogata, T. Kamino, K. Asayama, J. R. Cooper, and N. Athanassopoulou, J. Phys. Soc. Jpn. **62**, 2803 (1993).
[30] J. Korringa, Physica **16**, 601 (1950).
[31] T. Moriya, J. Phys. Soc. Jpn **18**, 516 (1963).
[32] G. E. Volovik, Pis'ma Zh. Eksp. Teor. Fiz. **58**, 457 (1993) [JETP Lett. **58**, 469 (1993)].
[33] M. Ichioka, K. Machida, N. Nakai, and P. Miranović, Phys. Rev. B **70**, 144508 (2004).
[34] N. Nakai, P. Miranović, M. Ichioka, and K. Machida, Phys. Rev. B **70**, 100503(R) (2004).
[35] Y. Masuda, Phys. Rev. **126**, 1271 (1962).